

A Modular Simulation Framework for Multidirectional Interaction Modeling in Cell Transmission Models

Zachary Feinstein^a Justin Plückerbaum^b

Stefan Weber^c

April 22, 2026

Abstract

Modeling multidirectional interactions in macroscopic flow simulations is challenging, as multiple concurrent streams must be represented consistently within individual simulation components. While the Cell Transmission Model (CTM) provides a scalable and interpretable framework, conventional formulations often lack a transparent internal representation of interaction effects within a cell. This paper introduces a graph-based internal cell notation in which each flow is uniquely defined by its origin and destination, so that all potentially interfering movements inside a cell become explicitly identifiable, enabling a modular integration of analytical and data-driven sending functions. Using pedestrian flow scenarios as a controlled testbed, we calibrate and compare a parametric interaction model and a machine-learning-based model under different demand levels using microsimulation-generated data. The results show that locally calibrated sending functions can accurately reproduce interaction dynamics and, when embedded into a network, yield globally consistent simulation behavior in systems with spatially localized interactions. The proposed framework demonstrates how explicit internal state representations and localized interaction structures support modular, data-driven calibration in CTM-based simulations, providing a transparent foundation for the simulation of complex multidirectional flow systems.

Keywords: simulation modeling; multidirectional interaction modeling; pedestrian flow simulation; hybrid modeling; cell transmission model

1 Introduction

Understanding and simulating interacting flows is a central challenge in many macroscopic simulation models, as multiple concurrent streams must be represented in a consistent and computationally efficient manner. In the context of pedestrian dynamics, this challenge is particularly pronounced in open spaces such as transit hubs, stadiums, or urban centers, as well as in evacuation scenarios, where several intersecting and opposing streams coexist, making them a frequent subject of simulation-based studies in the modeling and simulation literature.^{1,2} A wide range of modeling approaches has been developed to capture pedestrian movement across different spatial

^aStevens Institute of Technology, School of Business, Hoboken, NJ 07030, USA, email: zfeinste@stevens.edu.

^bLeibniz Universität Hannover, House of Insurance & Institute of Actuarial and Financial Mathematics, Welfengarten 1, 30167 Hannover, Germany, email: justin.plueckebaum@insurance.uni-hannover.de

^cLeibniz Universität Hannover, House of Insurance & Institute of Actuarial and Financial Mathematics, Welfengarten 1, 30167 Hannover, Germany, email: stefan.weber@insurance.uni-hannover.de

and temporal scales.³ Microscopic models, such as the Social Force Model⁴ or cellular automata,⁵ reproduce detailed local interactions and emergent collective patterns but often come with considerable computational cost. Macroscopic approaches, by contrast, describe movement in terms of aggregate quantities such as density and flow, offering greater scalability and interpretability.

Among macroscopic models, the Cell Transmission Model (CTM)^{6,7} provides a particularly attractive balance between computational efficiency, transparency, and theoretical grounding. However, when applied to pedestrian dynamics, CTM encounters a fundamental modeling challenge: unlike vehicular traffic, where links predominantly carry unidirectional flow, a single pedestrian cell must simultaneously accommodate several interacting streams. Existing extensions to bidirectional and multidirectional CTM formulations^{8,9} address this issue to some extent, yet they often represent the internal flow structure in an ad hoc manner by specifying only the origin of each stream. In environments with multiple possible exits, this is insufficient, as the destination of a flow is equally important for determining interaction patterns.^{10,11} Without jointly encoding both origin and destination, internal flow relations remain ambiguous, and interaction effects become difficult to model in a consistent and modular way.

Building on this insight, we introduce a graph-based internal cell notation that explicitly represents directional flows within a CTM cell. Each flow is uniquely characterized by its origin, current location, and destination, yielding a fully specified internal interaction structure. This explicit representation provides the basis for formulating, calibrating, and exchanging local interaction models in a modular manner. A preliminary version of the notation was outlined in an earlier preprint.¹²

Using this framework, we investigate whether CTM sending functions can be specified or learned locally at the site of pedestrian interactions without compromising global simulation consistency. Pedestrian flows provide a suitable testbed for this investigation, as interaction effects are predominantly confined to shared cells. This contrasts with vehicular traffic, where braking, acceleration, and spillback effects induce non-local dependencies across multiple cells. The central question is therefore not whether local interaction functions can be learned in isolation, but whether locally calibrated simulation components remain globally consistent when embedded into a networked CTM model. To examine this question under controlled conditions, we generate interaction scenarios using PTV VISSIM and compare a parametric analytical interaction model with a machine-learning-based alternative across different demand regimes. The results indicate that learned sending functions can reproduce the simulated interaction dynamics at the cell level and can be embedded into a CTM network without introducing unintended effects in adjacent cells.

The contributions of this paper are threefold. First, we introduce a graph-based internal representation for multidirectional CTM cells that explicitly encodes origin–location–destination relationships and resolves ambiguities in multidirectional CTM formulations. Second, we demonstrate how this representation enables a modular integration of analytical and data-driven sending functions within a consistent simulation framework. Third, we show that, for structurally localized pedestrian interactions, locally calibrated CTM components can be embedded into a network without compromising global simulation consistency.

The remainder of this paper is organized as follows. Section 2 introduces the graph-based notation and explains how it enables a consistent representation of multidirectional flows within CTM cells. Section 3 presents the experimental setup based on PTV VISSIM and reports the empirical results for the two data regimes. Section 4 concludes with implications for pedestrian modeling and outlines avenues for future research.

2 A Structured Cell Transmission Framework for Multidirectional Interactions

The Cell Transmission Model (CTM) provides a scalable framework for simulating the evolution of densities and flows over discretized space and time. In this paper, we use CTM as a macroscopic flow simulation framework in which each node $v \in V$ represents a spatial cell that may carry multiple concurrent directional streams. This is particularly relevant for applications, where a single cell can contain intersecting and opposing movements, for instance in shared spaces or interaction areas connecting several adjacent cells. To represent such multidirectional dynamics in a transparent and modular way, we introduce a structured notation that explicitly encodes origin–location–destination relationships within each cell. An initial sketch of the origin–location–destination idea was presented in an earlier preprint.¹² The present paper develops this idea into a fully structured CTM formulation, specifies its interaction semantics, and embeds it into a simulation-based calibration and evaluation workflow tailored to multidirectional interaction cells.

2.1 Related Work: Modeling Multidirectional Intersections

Modeling intersection cells poses a fundamental challenge in network-based flow simulations, as multiple potentially conflicting streams must be resolved within a confined spatial region. A common simplification is to represent the intersection areas as abstract connectors that balance inflow and outflow through capacity and demand constraints.¹³ While extensions of node-based models account for bidirectional flows and flow-dependent capacity reductions,^{9,14,15} they still treat the interaction area as an aggregate unit and abstract away internal spatial and directional interaction structures.

Several macroscopic pedestrian modeling approaches therefore represent intersection areas explicitly as spatial cells rather than point-like connectors, preserving traversal times and allowing interactions to be modeled at their physical location. Depending on the level of spatial resolution, this may range from representing an entire intersection as a single cell to discretizing it into multiple adjacent cells.^{8,16,17,18} However, when internal flows are characterized solely by their upstream origin, destination-dependent interactions remain implicit within the cell. In scenarios with multiple possible exits, this limitation becomes particularly apparent, as flows sharing the same origin but differing in destination may experience fundamentally different interactions within the same cell. As a consequence, the internal interaction structure of the cell is only partially specified, complicating a transparent and systematic formulation of interaction-dependent flow models.

To make these structures explicit, a structured internal flow representation is introduced in the following section. By uniquely labeling each flow by its origin, current location, and destination, the resulting interaction structure becomes unambiguous, transparent, and modular. This representation makes it possible to formulate sending functions that depend directly on the densities of all mutually interfering movements, thereby enabling consistent local calibration of interaction models. Figure 1 illustrates the notation for a representative interaction cell with four adjacent bidirectional connections, where the central cell comprises twelve distinct flow paths exhibiting different interaction patterns.

2.2 Internal Flow Representation of CTM Cells

To model movement in structured environments, we consider a set of cells or nodes V , each representing a spatial region (e.g., corridor section, plaza area, or stairwell). Adjacent cells are connected by a set of directed edges $E \subseteq V \times V$, which define feasible transitions between regions. The resulting directed graph $G = (V, E)$ is the traffic network under consideration. Movement streams traverse the graph and may interact locally within individual nodes. This is particularly

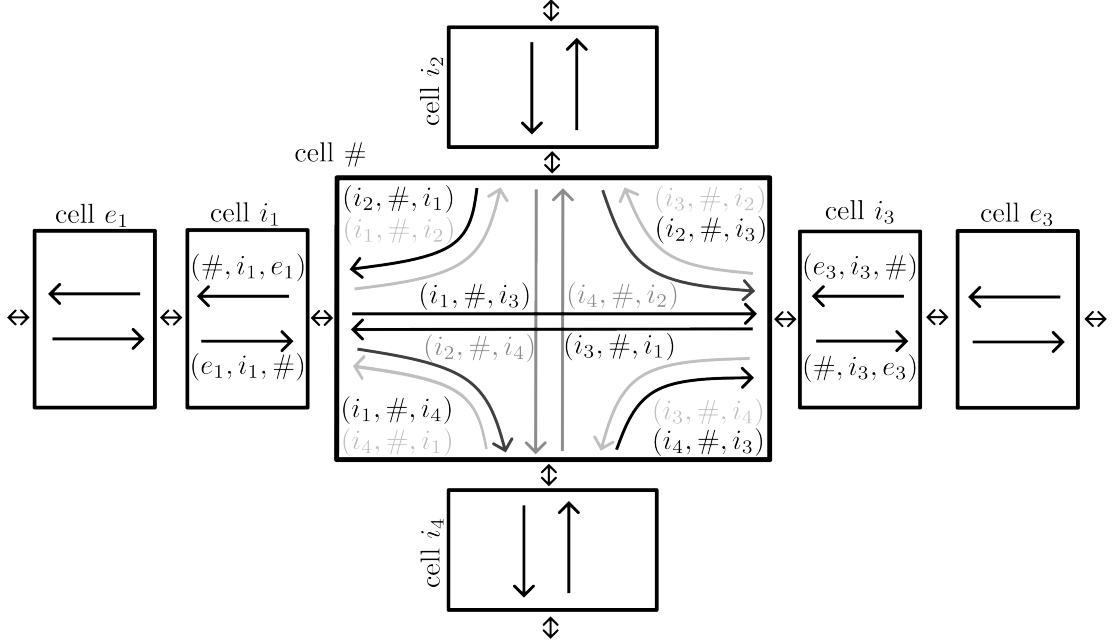


Figure 1: Graph-based origin–location–destination notation. Each path (u, v, w) represents a distinct directional flow through the cell, making internal interaction structures explicit.

relevant in pedestrian applications, where individuals are not constrained to predefined lanes and may traverse shared spaces toward different exits, allowing multiple directional movements to coexist within the same cell. To represent such situations explicitly, flows and their corresponding densities at a cell v are distinguished by both their preceding location $u \in \mathcal{I}(v)$ and their subsequent destination $w \in \mathcal{O}(v)$. Here, $\mathcal{I}(v) = \{v' \mid (v', v) \in E\}$ and $\mathcal{O}(v) = \{v' \mid (v, v') \in E\}$ denote the sets of upstream and downstream neighbors of v , respectively.

Flow Dynamics. The Cell Transmission Model (CTM) is employed here as a discrete-time macroscopic framework for flow simulation, where time is divided into uniform simulation steps indexed by $t = 0, 1, 2, \dots$. The time interval between consecutive simulation steps is denoted by ΔT [s]. This work focuses on pedestrian dynamics as a representative application of the proposed framework; the formalism extends straightforwardly to multiple interacting populations.

For each cell v and each movement route (u, v, w) through v , with $u \in \mathcal{I}(v)$ and $w \in \mathcal{O}(v)$, the pedestrian density at simulation step t is denoted by $\rho_{(u,v,w)}(t)$ and measured in [ped/m²]. The corresponding inflow and outflow rates during the time interval $(t \cdot \Delta T, (t + 1) \cdot \Delta T)$ are denoted by $q_{(u,v,w)}^{\text{in}}(t + 1)$ and $q_{(u,v,w)}^{\text{out}}(t + 1)$, respectively, with units [ped/s]. These represent the pedestrian flow rates crossing the boundary between adjacent spatial segments. The pedestrian density is updated at each simulation step according to the following conservation equation

$$\rho_{(u,v,w)}(t + 1) = \rho_{(u,v,w)}(t) + \frac{\Delta T}{A_v} \left(q_{(u,v,w)}^{\text{in}}(t + 1) - q_{(u,v,w)}^{\text{out}}(t + 1) \right), \quad (1)$$

where A_v [m²] denotes the area of cell v . This update equation ensures local conservation of pedestrians. Figure 2 illustrates an example of connected bidirectional cells in a pedestrian network. For clarity, time indices are omitted, and the figure focuses on the notation and the corresponding inflow and outflow streams.

To simulate a specific scenario, initial conditions and the dynamics of sources and sinks, namely external pedestrian inflow and outflow, must be specified exogenously. Such external flows can be incorporated in equation (1) but are omitted here for notational clarity. The feasible flows along a route (u, v, w) are constrained by the geometry of the spatial segment, the local

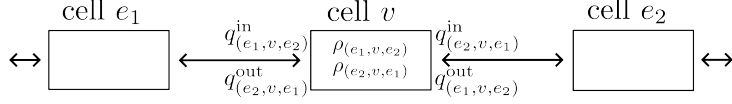


Figure 2: Connected cells (bidirectional pedestrian flow)

density of agents, and interactions with other streams passing through cell v . These constraints are captured by sending and receiving functions, which specify admissible flows based on the current local state. The allocation of realized flows is governed by additional interaction rules.

Sending and Receiving Functions. The following discussion introduces general supply and demand constraints, under which local densities in the CTM jointly constrain inflow and outflow along each path.

Consider a cell v at time t . Each directional movement through v is identified by an origin-cell-destination triple (u, v, w) and is associated with a density $\rho_{(u, v, w)}(t)$. Given the internal density state of cell v , outflows along each movement (u, v, w) during the next simulation step are constrained by a demand condition, formalized by the *sending function* $S_{(u, v, w)}$. This function represents the potential flow generated by traffic participants currently present in the cell that would be able to leave along this movement during the next simulation step if sufficient free space is available in the subsequent cell w . In this sense, the sending function captures the *demand for space* in the downstream cell w , or equivalently, the *flow that may be sent* out of cell v along the route (u, v, w) . Due to interactions between concurrent movements within a cell, the admissible outflow of a movement may depend on the full internal density state of the cell. Formally, for each movement (u, v, w) , the sending function is defined as

$$S_{(u, v, w)} : \begin{cases} \mathbb{R}_+^{\mathcal{J}(v) \times \mathcal{O}(v)} & \longrightarrow \mathbb{R}_+ \\ (\rho_{(u', v, w')})_{u' \in \mathcal{J}(v), w' \in \mathcal{O}(v)} & \longmapsto q_{(u, v, w)} \end{cases}.$$

As a basic feasibility condition, during one simulation step, the number of agents leaving cell v along (u, v, w) cannot exceed the number currently assigned to that movement. This is enforced by requiring that

$$S_{(u, v, w)}((\rho_{(u', v, w')}(t))_{u' \in \mathcal{J}(v), w' \in \mathcal{O}(v)}) \leq \frac{A_v}{\Delta T} \rho_{(u, v, w)}(t), \quad (2)$$

where A_v denotes the area of cell v .

The sending function thus provides an upper bound on the admissible outflow along movement (u, v, w) during the time interval $(t\Delta T, (t+1)\Delta T)$,

$$q_{(u, v, w)}^{\text{out}}(t+1) \leq S_{(u, v, w)}((\rho_{(u', v, w')}(t))_{u' \in \mathcal{J}(v), w' \in \mathcal{O}(v)}). \quad (3)$$

Examples of specific sending function formulations are provided in the following section.

While sending functions constrain what may leave a cell, inflows are constrained by a complementary supply condition. The supply constraint is formalized by the *receiving function* R , which specifies the maximum total inflow rate that a movement or a cell can accommodate during the next simulation step, given its current occupancy and spatial capacity. Accordingly, the receiving function represents the *supply of space* within the cell, or equivalently, the *flow that may be received*. Unlike the classical CTM, where each cell typically carries a single aggregate flow, the proposed framework explicitly represents multiple directional movements within the same cell. As in standard CTM merge models, multiple movements may compete for limited receiving capacity within a shared space. This leads to different modeling choices depending on

how this shared capacity is represented.

One possibility is to impose receiving constraints separately for each movement (u, v, w) , thereby bounding the corresponding inflow individually. Since movements may share physical space, these bounds may depend on the full internal density state of the cell. Formally, this yields a set of receiving constraints

$$R_{(u,v,w)} : \begin{cases} \mathbb{R}_+^{\mathcal{I}(v) \times \mathcal{O}(v)} & \longrightarrow \mathbb{R}_+ \\ (\rho_{(u',v,w')})_{u' \in \mathcal{I}(v), w' \in \mathcal{O}(v)} & \mapsto q_{(u,v,w)} \end{cases},$$

that bound the corresponding inflows according to

$$q_{(u,v,w)}^{\text{in}}(t+1) \leq R_{(u,v,w)}((\rho_{(u',v,w')}(t))_{u' \in \mathcal{I}(v), w' \in \mathcal{O}(v)}).$$

In addition, the sum of all movement-wise receiving constraints within a cell is required to be bounded by the available space of that cell. In this formulation, each movement is subject to its own receiving constraint, and unused capacity associated with one movement cannot be reassigned to others.

Alternatively, a joint receiving constraint can be imposed for all inflows into a cell. Accordingly, the receiving function for cell v is defined as

$$R_v : \begin{cases} \mathbb{R}_+^{\mathcal{I}(v) \times \mathcal{O}(v)} & \longrightarrow \mathbb{R}_+ \\ (\rho_{(u',v,w')})_{u' \in \mathcal{I}(v), w' \in \mathcal{O}(v)} & \mapsto R_v \end{cases},$$

and bounds the sum of all inflows into cell v according to

$$\sum_{u \in \mathcal{I}(v), w \in \mathcal{O}(v)} q_{(u,v,w)}^{\text{in}}(t+1) \leq R_v((\rho_{(u',v,w')}(t))_{u' \in \mathcal{I}(v), w' \in \mathcal{O}(v)}). \quad (4)$$

This approach allows unused capacity from one movement to be utilized by others and provides a flexible and compact representation of shared-space interactions. To obtain a unique set of realized flows when multiple inflows compete for limited capacity, an additional allocation rule is required that specifies how the available space is shared among competing movements. A common choice is to distribute capacity proportionally to the individual demand levels of the inflows, as proposed by Asano.⁸

Between these two extremes, hybrid formulations are also possible, combining movement-specific receiving constraints with joint capacity constraints for selected subsets of movements.

Sending and receiving functions are not necessarily constant over time, but may vary in response to dynamic factors such as weather conditions, temporary obstructions, or changes in agent composition (e.g., commuters, tourists, or event-related crowds), each associated with different movement characteristics. The proposed framework allows both functions to depend on additional state variables, thereby enabling the representation of such time-varying conditions within flow simulations.

Multiple successor nodes. In cases where multiple downstream movements are possible, we denote by $f_{(x,u,v) \rightarrow w}(t+1) \geq 0$ the fraction of pedestrians on (x, u, v) directed toward a specific outgoing link $w \in \mathcal{O}(v)$. These fractions satisfy

$$\sum_{w \in \mathcal{O}(v)} f_{(x,u,v) \rightarrow w}(t+1) = 1.$$

This yields the following flow conservation relationship:

$$q_{(u,v,w)}^{\text{in}}(t+1) = \sum_{x \in \mathcal{I}(u)} f_{(x,u,v) \rightarrow w}(t+1) \cdot q_{(x,u,v)}^{\text{out}}(t+1). \quad (5)$$

Optimization-Based Characterization of Flow Allocation. The realized flows at each simulation step can be interpreted as the solution of a linear programming (LP) problem that maximizes total throughput, subject to sending and receiving constraints. The resulting optimization problem may admit multiple optimal solutions, particularly when several inflows compete for limited receiving capacity. In these situations, additional interaction rules are required to obtain a unique and behaviorally meaningful solution. Tampère et al. introduce the concept of Supply Constraint Interaction Rules (SCIR) to resolve such ambiguities, for example by enforcing first-in-first-out (FIFO) principles when competing flows share limited space.¹⁴ In addition, node supply constraints may be imposed to capture further reductions in admissible flows caused by internal mechanisms such as signaling, priority rules, or conflicts occurring within the node. A realistic node or cell model therefore corresponds to solving the same flow maximization problem subject to these additional constraints, which encode both physical and behavioral considerations.

Accordingly, the outflows $q_{(u,v,w)}^{\text{out}}(t+1)$ can be characterized as solutions of the following per-step optimization problem:

$$\text{argmax} \sum_{v \in V} \sum_{u \in \mathcal{I}(v), w \in \mathcal{O}(v)} q_{(u,v,w)}^{\text{out}}(t+1) \quad (6)$$

subject to, for all $v \in V$, $u \in \mathcal{I}(v)$, $w \in \mathcal{O}(v)$:

- $q_{(u,v,w)}^{\text{out}}(t+1) \geq 0$,
- $q_{(u,v,w)}^{\text{out}}(t+1) \leq S_{(u,v,w)}((\rho_{(u',v,w')}(t))_{u' \in \mathcal{I}(v), w' \in \mathcal{O}(v)})$,
- $q_{(u,v,w)}^{\text{in}}(t+1) = \sum_{x \in \mathcal{I}(u)} f_{(x,u,v) \rightarrow w}(t+1) q_{(x,u,v)}^{\text{out}}(t+1)$,

together with one of the following receiving constraint specifications:

(R1) Movement-wise receiving constraints:

$$q_{(u,v,w)}^{\text{in}}(t+1) \leq R_{(u,v,w)}((\rho_{(u',v,w')}(t))_{u' \in \mathcal{I}(v), w' \in \mathcal{O}(v)}), \quad \forall v \in V, u \in \mathcal{I}(v), w \in \mathcal{O}(v).$$

(R2) Joint receiving constraints:

$$\sum_{u \in \mathcal{I}(v), w \in \mathcal{O}(v)} q_{(u,v,w)}^{\text{in}}(t+1) \leq R_v((\rho_{(u',v,w')}(t))_{u' \in \mathcal{I}(v), w' \in \mathcal{O}(v)}), \quad \forall v \in V.$$

To ensure uniqueness, additional interaction rules such as SCIR or node supply constraints must be specified.

Remark (Splitting the global flow allocation problem). *The global flow allocation problem (6) can be decomposed into smaller, independent subproblems depending on how receiving constraints are defined.*

If receiving constraints are specified separately for each movement, then all outflows leading into the same movement are determined jointly, as they share the same receiving constraint, while outflows associated with different movements can be computed independently. As a result, the global flow allocation problem decomposes into independent subproblems of the form

$$\text{argmax} \sum_{a \in \mathcal{I}(b)} q_{(a,b,c)}^{\text{out}}(t+1),$$

for each $c \in V, b \in \mathcal{O}(c)$ subject to the corresponding constraints.

If, in contrast, a joint receiving constraint is imposed at the level of a cell, then all inflows into that cell are coupled through a common capacity constraint. In this case, the global flow allocation problem no longer decomposes into independent movement-wise subproblems, but can instead be decomposed into independent cell-wise optimization problems, in which all outflows leading into the same cell are determined jointly. Accordingly, instead of solving the global problem (6), we may solve

$$\operatorname{argmax} \sum_{b \in \mathcal{I}(c)} \sum_{a \in \mathcal{I}(b)} q_{(a,b,c)}^{\text{out}}(t+1),$$

for each $c \in V$ subject to the corresponding constraints.

In the special case of a chain of cells with exactly one inflow and one outflow per cell, the optimization problem collapses to the classical CTM formulation, in which the outflow is determined as the minimum of the sending function and the receiving function associated with the cell transition and can be solved independently for each outflow variable.

Sequential Simulation Procedure. At each simulation step $t+1$, the sending and receiving functions are first evaluated for every cell based on the current density state. Given these constraints, the corresponding maximization problems (e.g., (6)) are solved to determine the admissible outflows, from which the resulting inflows follow via the relationship (5). Finally, the densities in all cells are updated according to the conservation equation (1).

2.3 Examples of Multidirectional Interaction Cells in Pedestrian Networks

Our general framework provides a transparent way to represent and parameterize interactions within different types of cells. Below, a set of representative cell archetypes is introduced to illustrate how sending and receiving functions can be specified to capture interactions between multiple movement directions. These examples are not intended as exhaustive or prescriptive model specifications, but rather serve to illustrate how typical interaction patterns can be instantiated within the proposed framework using commonly adopted functional forms. For clarity and notational consistency, the cell under consideration is denoted by $\#$ in all examples. The three representative configurations are depicted in Figure 3.

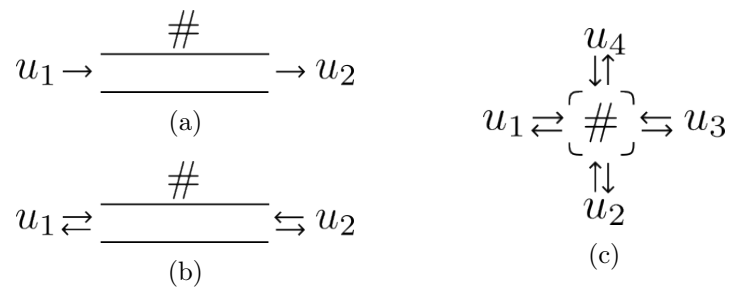


Figure 3: Representative pedestrian cell configurations: (a) unidirectional segment, (b) bidirectional interface, (c) pedestrian square with four connected directions

Unidirectional Segment. We consider a single unidirectional movement from an upstream cell u_1 to a downstream cell u_2 through cell $\#$. In this configuration, no interactions between different walking directions occur, and the model reduces to the classical CTM formulation for a single flow. In practice, such situations are commonly modeled using simple, piecewise-linear sending and receiving functions, as they admit a clear physical interpretation and depend only on a small

number of parameters. One possible specification of the sending and receiving functions is given by

$$S_{(u_1, \#, u_2)}(\rho_{(u_1, \#, u_2)}) = \min \left\{ q_{(u_1, \#, u_2)}^{\max}, f_{(u_1, \#, u_2)}^{\text{free}}(\rho_{(u_1, \#, u_2)}) \right\},$$

$$R_{\#}(\rho_{(u_1, \#, u_2)}) = \min \left\{ q_{(u_1, \#, u_2)}^{\max}, w(\rho_{(u_1, \#, u_2)}^{\max} - \rho_{(u_1, \#, u_2)}) b_{u_1, \#} \right\}.$$

Here, $q_{(u_1, \#, u_2)}^{\max}$ denotes the maximum admissible flow [ped/s], $\rho_{(u_1, \#, u_2)}^{\max}$ the maximum pedestrian density [ped/m²], w the backward wave speed [m/s], and $b_{u_1, \#}$ the width of the upstream interface [m]. A simple linear free-flow relationship is given by

$$f_{(u_1, \#, u_2)}^{\text{free}}(\rho_{(u_1, \#, u_2)}) = v_{(u_1, \#, u_2)}^{\text{free}} \cdot \rho_{(u_1, \#, u_2)} \cdot b_{\#, u_2},$$

where $v_{(u_1, \#, u_2)}^{\text{free}}$ denotes the free-flow walking speed [m/s]. More general functional forms, including higher-order polynomials or other nonlinear relationships, can be employed if warranted by empirical observations.

Bidirectional Interfaces. Consider a bidirectional cell $\#$ with opposing movements $(u_1, \#, u_2)$ and $(u_2, \#, u_1)$. In this case, pedestrian streams interact directly by sharing physical space, necessitating sending and receiving functions that account for mutual interference between opposing flows.¹⁹ A possible concretization of the *sending function* for the movement $(u_1, \#, u_2)$ is

$$S_{(u_1, \#, u_2)}(\rho_{(u_1, \#, u_2)}, \rho_{(u_2, \#, u_1)}) = \min \left\{ q_{(u_1, \#, u_2)}^{\max}, f_{(u_1, \#, u_2)}^{\text{free}}(\rho_{(u_1, \#, u_2)}) \cdot f_{(u_1, \#, u_2)}^{\text{red}}(\rho_{(u_1, \#, u_2)}, \rho_{(u_2, \#, u_1)}) \right\}.$$

In contrast to the unidirectional case, the potential outflow is impeded by an opposing stream. This effect is captured by a reduction function $f_{(u_1, \#, u_2)}^{\text{red}}(\rho_{(u_1, \#, u_2)}, \rho_{(u_2, \#, u_1)})$, which modulates the free-flow sending capacity to account for interference with the opposing stream. For physical consistency, the reduction function is required to satisfy $f_{(u_1, \#, u_2)}^{\text{red}}(\cdot) = 1$ in the absence of opposing flow, i.e., when $\rho_{(u_2, \#, u_1)} = 0$, so that the sending function reduces to the free-flow relationship introduced for the unidirectional case. Moreover, the resulting sending function is required to be non-increasing in the density of the opposing flow, ensuring that admissible outflow is reduced as counterflow interference increases.

As an illustrative example, the reduction function may be specified following Lilasathapornkit and Saberi²⁰ as

$$f_{(u_1, \#, u_2)}^{\text{red}}(\rho_{(u_1, \#, u_2)}, \rho_{(u_2, \#, u_1)}) = \frac{1}{1 - \frac{\rho_{(u_1, \#, u_2)}}{\rho_{(u_1, \#, u_2)} + \rho_{(u_2, \#, u_1)}}} \quad \text{or}$$

$$f_{(u_1, \#, u_2)}^{\text{red}}(\rho_{(u_1, \#, u_2)}, \rho_{(u_2, \#, u_1)}) = \left(\frac{\rho_{(u_1, \#, u_2)}}{\rho_{(u_1, \#, u_2)} + \rho_{(u_2, \#, u_1)}} \right)^{\gamma}, \quad \gamma > 0,$$

where γ is a calibration parameter controlling the sensitivity to counterflow.

Alternative functional forms may be employed if suggested by empirical observations or expert knowledge. For example, Moustaid and Flötteröd propose a nonlinear sending function that applies in regimes where both the density and the counterflow density remain below their respective critical values.⁹

The collective *receiving function* may, for example, be specified as

$$R_{\#}(\rho_{(u_1, \#, u_2)}, \rho_{(u_2, \#, u_1)}) = \min \left\{ q_{\#}^{\max}, w \cdot ((\rho_{\#}^{\max} - \rho_{(u_1, \#, u_2)}) - \rho_{(u_2, \#, u_1)}) \cdot (b_{u_1, \#} + b_{\#, u_2}) \right\}.$$

To obtain a unique set of realized flows when both directions compete for limited capacity, an additional allocation rule must be specified. A common choice is to distribute the available receiving capacity proportionally to the density ratios of the competing streams; if one direction does not fully utilize its assigned share, the remaining capacity becomes available to the

opposing flow. This formulation allows the effective available space and admissible inflow to adapt dynamically to the relative densities of the two directions, thereby providing a realistic macroscopic representation of pedestrian counterflow interactions.

A brief comparison with bidirectional vehicular traffic highlights the specificity of the pedestrian case. In road traffic, bidirectional links are typically represented by separate lanes, so that opposing streams do not share physical space and can be modeled independently using distinct sending and receiving functions. As a result, no explicit space allocation mechanism is required. More complex vehicular configurations are also possible, for example when straight-moving traffic interacts with opposing left-turning vehicles. Such interactions are commonly modeled by capacity reductions and, in some cases, by reductions in effective free-flow speed as a function of the conflicting flow.^{21,22} While local calibration of more detailed vehicular interaction functions is technically feasible, these models generally do not generalize correctly at the network level. Nonlocal effects such as braking, acceleration, and spillbacks propagate into neighboring cells, so that globally consistent behavior requires additional constraints on adjacent links.

Pedestrian Squares. Bidirectional interfaces can be generalized in a straightforward manner to settings with multiple interacting directions. A pedestrian square with n bidirectional entries and exits is represented by a cell $\#$ with $\mathcal{I}(\#) = \mathcal{O}(\#) = \{u_1, \dots, u_n\}$.

For a specific movement $(u_i, \#, u_j)$ with $u_i \neq u_j$, the *sending function* may, for example, be specified as

$$S_{(u_i, \#, u_j)} \left(\left(\rho_{(u_k, \#, u_l)} \right)_{\substack{u_k \in \mathcal{I}(\#), \\ u_l \in \mathcal{O}(\#)}} \right) = \min \left\{ q_{(u_i, \#, u_j)}^{\max}, f_{(u_i, \#, u_j)}^{\text{free}} \left(\rho_{(u_i, \#, u_j)} \right) \cdot f_{(u_i, \#, u_j)}^{\text{red}} \left(\left(\rho_{(u_k, \#, u_l)} \right)_{\substack{u_k \in \mathcal{I}(\#), \\ u_l \in \mathcal{O}(\#)}} \right) \right\}.$$

Moreover, the reduction function must evaluate to one when the considered movement is the only active flow in the cell, that is, when all other directional densities are zero. For physical consistency, the resulting sending function must be non-increasing in each density component corresponding to an interfering movement, for any fixed density of the considered direction.

A possible formulation of the collective *receiving function* is

$$R_{\#} \left(\left(\rho_{(u_k, \#, u_l)} \right)_{\substack{u_k \in \mathcal{I}(\#), \\ u_l \in \mathcal{O}(\#)}} \right) = \min \left\{ q_{\#}^{\max}, w \cdot \left(\left(\rho_{\#}^{\max} - \sum_{\substack{u_k \in \mathcal{I}(\#), \\ u_l \in \mathcal{O}(\#)}} \rho_{(u_k, \#, u_l)} \right) \cdot \sum_{u_k \in \mathcal{I}(\#)} b_{u_k, \#} \right) \right\}.$$

These examples illustrate how explicitly encoding origin–location–destination relationships enables transparent and modular representations of multidirectional interaction structures within a single cell, while allowing for flexible, application-specific specification of interaction functions.

3 Calibration Study in a Controlled Microsimulation Setting

While the previous sections focused on the theoretical formulation of the Cell Transmission Model (CTM) and illustrative analytical examples of sending and receiving functions defined on origin–location–destination paths, practical simulation applications require these relationships to be calibrated from data. We therefore investigate the calibration of local sending functions for a representative interaction cell, using microsimulation as a controlled experimental environment in which the internal directional flow state of each movement is explicitly observable. Microsimulation-generated data are used to systematically explore the interaction state space under controlled and reproducible conditions. This allows us to assess the stability of locally calibrated interaction functions and to examine whether such components can be composed into a globally consistent CTM network without introducing unintended coupling effects. The calibration study in this section relies on the explicit origin–location–destination state representation

introduced above. Without it, local interaction calibration would be ill-posed, since distinct interaction patterns would map to identical internal states.

Two approaches for modeling local interactions between multiple pedestrian streams within a shared cell are compared: (i) an analytical formulation based on explicit parametric functions, and (ii) a data-driven approach that infers the same relationship from data generated by the microsimulator PTV VISSIM.

3.1 Microsimulation Setup

The microsimulation setup is deliberately designed as a controlled experimental environment to generate reproducible interaction patterns for methodological evaluation. Parameter choices are not intended to increase behavioral realism, but to amplify and systematically vary local interaction effects relevant for calibration. All microscopic experiments were conducted using PTV VISSIM 2025, configured with the default pedestrian dynamics unless stated otherwise.

Experimental Setup. To evaluate the two modeling approaches under controlled and reproducible conditions, we designed a simplified pedestrian intersection scenario implemented in PTV VISSIM (Figure 4). The test network consists of four entry links, each followed by two unidirectional cells before merging into a central interaction zone where all streams intersect. Downstream of the crossing, each exit link again contains two unidirectional cells. Each cell (including the interaction cell) has a uniform length of 12.5 m, which pedestrians must fully traverse in order to advance to the next segment. All regular cells have a width of 2.1m. To isolate local interaction effects, we assume that no downstream spillbacks occur beyond the intersection; pedestrians can exit the system freely at the downstream boundaries. Within the central crossing area, defined as a circular region with a diameter of 6 m, the default walking behavior parameters were modified to increase the intensity of interactions. Specifically, the relaxation time τ was increased from 0.40 to 0.50s, the lateral interaction range parameter B_{SocIso} from 0.20 to 0.24m, and the noise term from 1.20 to 1.50. Strengthening these parameters increases behavioral variability and interaction sensitivity within the conflict zone, thereby generating richer and more informative trajectories for subsequent model calibration. All simulations were conducted exclusively with pedestrians of type IMO-M 30-50, ensuring homogeneous agent characteristics across all scenarios. Each simulation run covers a period of 30 min, with flow and density values recorded every 10s for all cells. This temporal resolution corresponds to the time a pedestrian requires to traverse one CTM cell under free-flow conditions, thereby allowing a consistent temporal discretization between the microscopic simulation and the CTM representation.

Scenario Design and Data Regimes. Two distinct data regimes were designed to examine how the coverage and granularity of the observed state space affect calibration stability and out-of-sample generalization. Rather than representing different real-world demand conditions, the regimes serve to systematically vary the diversity of interaction configurations available for model identification. The *small-data regime* is constructed from pedestrian inflow rates at the four entries (in_1, in_2, in_3, in_4) selected from the discrete set $\{0, 2000, 4000, 6000\}$ ped/h, under the global constraint $\sum_{i=1}^4 in_i \leq 14,000$. This yields 190 feasible inflow combinations. This regime represents a sparse sampling of the interaction state space and is intended to test calibration robustness under limited observational diversity. A separate set of test scenarios was generated analogously using inflow levels from $\{0, 3000, 5000\}$ ped/h, again respecting the overall demand constraint.

The *large-data regime* increases the resolution of demand levels in order to provide a denser sampling of interaction configurations, thereby enabling a more detailed assessment of model generalization behavior. In this regime, inflow rates are selected from $\{0, 1000, 2000, 3000,$

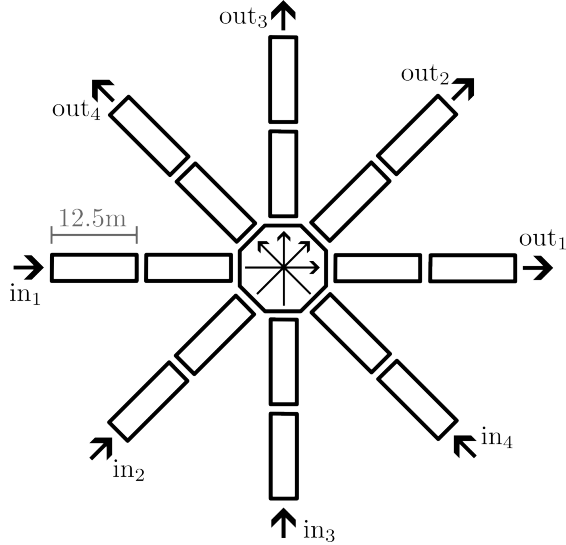


Figure 4: Design of the Case Study

4000, 5000, 6000} ped/h under the same global constraint, resulting in 1746 unique demand configurations. For model development, 70% of the aggregated observations were randomly assigned to the training set, while the remaining 30% were reserved for out-of-sample evaluation.

For both regimes, each scenario was simulated 20 times, and averaged observations were used for calibration and validation in order to reduce stochastic noise and isolate systematic interaction effects. Densities and flows of all cells were recorded at 10 s intervals.

All scenarios were designed to avoid upstream congestion or spillbacks that could result from oversaturation of the intersection area, which would otherwise produce unrealistic results in the microscopic simulation. Under these conditions, the calibration exclusively targets the sending function, while the *receiving function* remains inactive and does not constrain the system dynamics. This restriction provides a controlled and analytically transparent environment for assessing whether local flow relationships can be learned reliably from data. The focus on isolated sending dynamics thus constitutes a necessary first step before extending the approach to more complex configurations in which sending and receiving mechanisms jointly determine system performance.

Data Quality and Consistency. To assess the internal consistency of the simulation data, we first consider scenarios without interacting pedestrian streams. In these cases, pedestrians exhibit nearly identical free-flow travel times across all directions of the network, confirming that the microsimulation produces uniform baseline behavior in the absence of interactions.

Averaging over 20 independent simulation replications further yields a highly stable basis for subsequent calibration and validation. An analysis of travel-time variability in the large-data regime shows that OD-specific travel times measured in individual simulation runs deviate only marginally from their corresponding scenario means. Across all scenarios and origin–destination pairs in the large-data regime, the mean absolute percentage error (MAPE) between the average travel time observed in a single run and the corresponding 20-run average is approximately 0.73%, while even the upper 5% quantile of deviations remains below 2%.

This low level of stochastic dispersion indicates that the simulated interaction outcomes cluster tightly around their expected values. Consequently, the use of averaged observations provides a robust and reproducible representation of the underlying simulation behavior, suitable for isolating systematic interaction effects in the subsequent calibration and evaluation steps.

3.2 Interaction Model Specifications

To compare analytical and data-driven representations of pedestrian interactions within the CTM framework, a reference sending function is first derived from the microsimulation data. This empirical baseline is applied to all cells outside the central interaction area in order to ensure a consistent and data-aligned representation of free-flow and unidirectional movements throughout the network. For each 10s interval of the PTV VISSIM experiments, densities and corresponding outflows are recorded for all directional movements. Based on these observations, a third-degree polynomial is fitted by minimizing the root mean squared error (RMSE) between predicted and observed outflows. While a second-degree polynomial already achieves a comparable coefficient of determination, the third-degree specification is retained due to its lower approximation error in terms of RMSE, which is more relevant for stable flow propagation within the CTM. Rather than representing a behavioral law, the resulting polynomial provides a smooth and reproducible approximation of the flow-density relationship observed in the microsimulation and serves as a standardized simulation component for non-interacting cells. Consistent with the previously defined training-test split, the out-of-sample RMSE differs by less than 1.7% from the in-sample value, indicating that the selected polynomial degree yields a stable approximation without signs of overfitting. The resulting polynomial coefficients obtained from the RMSE minimization are reported in Table 1.

Data Regime	b_1	b_2	b_3	RMSE	R^2
small	25.2049	-17.1462	7.5251	0.2478	0.9983
large	25.9977	-16.5198	7.1222	0.2394	0.9979

Table 1: Coefficients of the third-degree polynomial sending function $S(\rho) = b_1\rho^1 + b_2\rho^2 + b_3\rho^3$ estimated from microsimulation training data for non-interacting cells, used as a standardized reference component outside the interaction area.

Simplified Analytical Interaction Model. This approach specifies interaction effects through explicit parametric functions that map directional density states to admissible outflows, following the structured formulation introduced in the previous section. These analytical specifications provide transparent and interpretable local interaction rules and ensure that basic physical and capacity constraints are respected. However, as the number of concurrent movement directions increases, the complexity of such models grows rapidly, since each additional stream introduces further interaction terms and calibration parameters. This limits scalability and motivates the comparison with data-driven alternatives in settings with richer interaction patterns.

We consider a deliberately simplified parametric interaction structure in which all interfering pedestrian streams are assumed to exert a symmetric influence on the movement under consideration. For a given directional movement $(u_i, \#, u_j)$, the sending function is specified as

$$S_{(u_i, \#, u_j)} \left(\left(\rho_{(u_k, \#, u_l)} \right)_{\substack{u_k \in \mathcal{S}(\#), \\ u_l \in \mathcal{O}(\#)}} \right) = \min \left\{ q_{(u_i, \#, u_j)}^{\max}, f^{free}(\rho_{(u_i, \#, u_j)}) \cdot f^{red}(\rho_{(u_i, \#, u_j)}, \rho_{\overline{(u_i, \#, u_j)}}) \right\}.$$

where $\rho_{\overline{(u_i, \#, u_j)}}$ denotes the sum of densities of all flows that interact with $(u_i, \#, u_j)$ inside the cell.

The free-flow component is approximated by a third-degree polynomial,

$$f^{free}(\rho_{(u_i, \#, u_j)}) = a_1 * \rho_{(u_i, \#, u_j)} + a_2 * \rho_{(u_i, \#, u_j)}^2 + a_3 * \rho_{(u_i, \#, u_j)}^3,$$

while interaction effects are captured by a reduction term of the form

$$\begin{aligned}
f^{red}(\rho_{(u_i, \#, u_j)}, \overline{\rho_{(u_i, \#, u_j)}}) &= 1 + g_1(\rho_{(u_i, \#, u_j)}) * \overline{\rho_{(u_i, \#, u_j)}} + g_2(\rho_{(u_i, \#, u_j)}) * \overline{\rho_{(u_i, \#, u_j)}^2}, \\
g_1(\rho_{(u_i, \#, u_j)}) &= g_{1,1} + g_{1,2} * \rho_{(u_i, \#, u_j)} + g_{1,3} * \rho_{(u_i, \#, u_j)}^2, \\
g_2(\rho_{(u_i, \#, u_j)}) &= g_{2,1} + g_{2,2} * \rho_{(u_i, \#, u_j)} + g_{2,3} * \rho_{(u_i, \#, u_j)}^2.
\end{aligned}$$

The reduction function is constrained to values not exceeding one and equals one in the absence of conflicting flows, ensuring that the model reduces to the free-flow relationship when no interactions are present.

The parameters of the analytical interaction model are estimated by minimizing the mean squared error between predicted and observed outflows for each directional movement, given the corresponding density states of all interacting streams within the interaction cell. The estimation is subject to the constraint that the resulting product of the free-flow term and the reduction term, is non-increasing in the aggregate density of all interfering movements for any fixed density of the considered direction, over the range of density states relevant for calibration and subsequent validation.

To ensure that the resulting sending functions remain compatible with stable network simulation, underestimation errors, meaning cases in which the predicted outflow falls below the observed value, are penalized more strongly than overestimation errors. This asymmetric weighting reduces the risk of systematically restricting admissible flows in downstream cells and supports consistent flow propagation when the calibrated functions are embedded into the CTM network.

Data Regime	a_1	a_2	a_3	RMSE
small	118.8272	-313.5473	743.1899	0.1321
large	116.7051	-280.7368	634.1721	0.1250

Table 2: Fixed free-flow coefficients used in the analytical interaction model.

Data Regime	g_1			g_2			RMSE	
	$g_{1,1}$	$g_{1,2}$	$g_{1,3}$	$g_{2,1}$	$g_{2,2}$	$g_{2,3}$	train	test
small	-1.1471	12.7083	-41.0728	0.7699	-21.6432	67.3856	0.4751	0.4824
large	-0.9851	10.0293	-31.7092	0.3790	-15.2141	44.1921	0.4241	0.4220

Table 3: Calibrated interaction parameters and predictive errors of the analytical model.

Data-Driven Interaction Model. As an alternative to explicit analytical specifications, a data-driven interaction model is constructed in which the sending function is learned directly from observed flow–density relationships in the microsimulation data. Within the proposed notation, this corresponds to replacing the analytical interaction kernel by a learned local mapping from the internal density state of a cell to its directional outflows, allowing nonlinear and higher-order interaction effects to be captured without prescribing a specific functional form.

The learning model is implemented using MATLAB’s `LSBoost` algorithm (`fitrensemble` with `Method=‘LSBoost’` and 300 boosting iterations). Gradient boosting is used as a flexible regression engine rather than as a behavioral or agent-based model, providing a smooth nonparametric approximation of the empirical interaction surface. The predictor variables consist of the directional densities of all interfering movement paths within the interaction cell (in the present case, three density variables corresponding to the three conflicting paths), observed at each 10, s interval, and the target variable is the corresponding directional outflow. Separate models are

trained for each movement direction, yielding a set of locally calibrated sending functions that are fully compatible with the CTM framework.

To ensure consistency with the analytical calibration, the regression loss is defined asymmetrically, assigning a higher weight to underestimation than to overestimation errors. The training procedure therefore proceeds iteratively. After an initial model is fitted, prediction errors are evaluated and used to update the asymmetric weighting of the loss function. A new model is then trained under the updated weights, and this process is repeated until changes in the learned sending functions fall below a predefined tolerance. This fixed-point iteration yields a regression model that balances empirical fit with network-level flow compatibility.

No-Interaction Baseline. This model serves as a baseline that neglects interaction effects entirely. It is structurally identical to the analytical formulation but assumes no interaction-induced reduction, i.e., the reduction term is fixed to $f^{red} \equiv 1$. This baseline is used to isolate the contribution of interaction modeling: by comparing its performance with the analytical and machine-learning models, we quantify the extent to which interaction effects improve predictive accuracy.

3.3 Simulation-Based Evaluation

The evaluation is designed to assess how well locally specified interaction models, whether analytical or data-driven, reproduce the flow behavior generated by the microsimulation when embedded into the CTM framework. The focus is not on matching real-world pedestrian dynamics, but on measuring the internal consistency, generalization, and stability of locally calibrated simulation components.

Performance is evaluated using movement-specific average travel times for the four origin-destination relations in each demand scenario. These travel times are derived from cumulative flow curves, which provide a robust representation of the temporal evolution of simulated flows. A key advantage of cumulative flows is that they preserve the temporal structure of deviations, thereby smoothing stochastic noise and highlighting systematic discrepancies between models. While the analysis is therefore reported in terms of travel times, these metrics implicitly integrate the full time-dependent flow behavior of the network and serve as compact and interpretable summaries of how different local interaction models propagate to the network level.

3.3.1 Local Interaction Model Behavior

In this local evaluation, the intersection cell is simulated as a stand-alone CTM component, driven by the time-varying inflows observed in the PTV VISSIM experiments at 10 s resolution. Unlike in the calibration phase, where densities and outflows are related in a purely static mapping, the learned or specified sending functions are here embedded into a recursive simulation loop: the outflow predicted in one time step, together with the inflow, determines the density in the next step, which in turn affects subsequent outflows. This setting therefore tests whether the locally calibrated interaction models remain stable and dynamically consistent when used as simulation components rather than as one-step regressors.

Table 4 reports the relative absolute travel-time errors for the three interaction models under both data regimes for the interaction cell. These errors reflect how accurately the locally specified sending functions reproduce the microsimulation-generated flow behavior under different calibration conditions.

Both the analytical and the data-driven interaction models substantially reduce the error compared to the no-interaction baseline, in-sample as well as out-of-sample. This confirms that explicitly modeling local interaction effects improves the ability of the CTM to reproduce the simulated interaction dynamics at the cell level.

In the small-data regime, the machine-learning model achieves the lowest in-sample errors, clearly outperforming the analytical formulation. This behavior is expected: with limited observations, a flexible learning model can adapt closely to the available data and capture fine-grained interaction patterns. However, this flexibility also induces overfitting, which becomes apparent in the out-of-sample results, where the analytical model performs more robustly.

In the large-data regime, this pattern reverses. With substantially broader coverage of the interaction state space, the machine-learning model learns a more stable representation of the local interaction structure and generalizes more reliably beyond the training data. As a result, it achieves consistently lower errors than the analytical model both in-sample and out-of-sample. This illustrates how data-driven interaction models transition from overfitting-prone approximators to reliable local simulation components as data availability increases.

Data Regime	Interaction Model	RAE (in-sample)				RAE (out-of-sample)			
		Mean Error	90th Perc.	95th Perc.	Worst 5%	Mean Error	90th Perc.	95th Perc.	Worst 5%
small	Analytical	4.49%	9.01%	10.22%	11.27%	4.45%	9.3357%	12.00%	12.40%
	ML	1.42%	2.80%	3.55%	4.87%	5.63%	12.33%	16.90%	19.73%
	No-Interaction	18.06%	34.44%	40.02%	42.80%	15.05%	32.10%	41.11%	41.51%
large	Analytical	3.95%	7.57%	8.50%	9.93%	3.90%	7.47%	8.51%	10.05%
	ML	2.01%	3.76%	4.56%	5.99%	2.25%	4.63%	5.89%	8.95%
	No-Interaction	18.95%	33.68%	38.18%	42.42%	19.11%	34.40%	38.55%	42.65%

Table 4: Local comparison of relative absolute travel-time errors across interaction models.

3.3.2 Network-Level Consistency

In the network-level evaluation, the locally calibrated interaction models are embedded into the full CTM network consisting of two standard cells upstream of the interaction area, the central interaction cell, and two standard cells downstream. As in the local experiment, time-varying inflow rates at a 10 s resolution are taken from the PTV VISSIM simulations, but here they enter the CTM network at the upstream boundary and propagate through all five cells. This setting therefore tests whether locally calibrated interaction models remain stable and consistent when coupled to surrounding CTM dynamics.

Table 5 reports the relative absolute travel-time errors for all models at the network level. Compared with the local interaction cell, global errors are systematically smaller. This is expected, since two non-interacting CTM cells are placed upstream and downstream of the interaction region, whose predictable dynamics attenuate the relative impact of local interaction mismatches on overall travel times.

More importantly, the qualitative ranking of the models is preserved at the network level. The interaction models that perform well locally also exhibit consistent behavior when embedded into the surrounding CTM network. This indicates that the locally calibrated sending functions do not introduce spurious or unstable effects in adjacent cells, but remain compatible with the global flow dynamics of the simulation.

This behavior relies on the structural locality of pedestrian interactions. Because interaction effects are confined to the shared interaction cell, the surrounding cells remain governed by their own sending and receiving functions. In contrast, vehicular traffic exhibits non-local coupling through braking, acceleration, and spillback effects, so that locally calibrated interaction functions would not remain valid when embedded into a larger network.

As in the local analysis, the machine-learning model trained on limited data exhibits overfitting: it achieves very low in-sample errors but generalizes less robustly than the analytical

model. In the large-data regime, however, the learned interaction model generalizes reliably and slightly outperforms the analytical formulation both locally and at the network level. This confirms that data-driven interaction models can serve as stable and accurate CTM components when sufficient coverage of the interaction state space is available.

Data Regime	Interaction Model	RAE (in-sample)				RAE (out-of-sample)			
		Mean Error	90th Perc.	95th Perc.	Worst 5%	Mean Error	90th Perc.	95th Perc.	Worst 5%
small	Analytical	1.10%	2.33%	2.92%	3.35%	1.61%	3.10%	4.25%	4.67%
	ML	0.43%	0.93%	1.16%	1.69%	1.78%	3.79%	4.92%	6.39%
	No-Interaction	4.27%	9.00%	11.48%	12.58%	3.76%	8.04%	12.36%	12.73%
large	Analytical	1.11%	2.28%	2.74%	3.27%	1.10%	2.24%	2.70%	3.24%
	ML	0.72%	1.53%	1.82%	2.23%	0.78%	1.59%	2.03%	2.84%
	No-Interaction	4.2334%	8.48%	10.47%	12.15%	4.26%	8.64%	10.38%	12.12%

Table 5: Global comparison of relative absolute travel-time errors across interaction models.

4 Conclusion

This paper introduced a structured graph-based notation for macroscopic flow simulations that enables a clear and unambiguous internal representation of multidirectional flows within individual CTM cells. By explicitly encoding origin–location–destination relationships, interaction structures inside a cell become uniquely defined rather than implicitly inferred. This representation is not merely a formal refinement, but a structural prerequisite for modular modeling and calibration of interaction mechanisms within cell-based simulation frameworks.

Building on this explicit state representation, which renders local interaction effects identifiable, we examined the feasibility of learning local sending functions for interacting pedestrian flows using microsimulation data. The results show that, for systems with spatially localized interaction effects, both analytical and data-driven local components can be identified with high stability and composed into a globally consistent network simulation, with data-driven models benefiting from increased coverage while analytical formulations provide a robust baseline under limited data.

The applicability of the proposed approach is strongest in settings characterized by spatially localized interactions and limited non-local effects, such as pedestrian movement in shared spaces. Conversely, domains dominated by long-range interactions or network-wide feedback mechanisms require additional structural constraints beyond local calibration.

Future research may extend the framework toward learning receiving functions, multi-cell interaction structures, robustness under congestion, and integration with empirical trajectory data. Beyond pedestrian modeling, the proposed notation provides a general template for designing modular interaction components in macroscopic simulation models whenever multiple directional flows coexist within a shared spatial unit.

Acknowledgements

The authors used AI-assisted tools (ChatGPT) to improve wording and grammar. All scientific content, interpretations, and conclusions were fully created, verified, and approved by the authors.

The authors gratefully acknowledge PTV VISSIM for providing a research software license that supported this study.

Statements and Declarations

Ethical considerations

There are no human participants in this article.

Consent to participate

Not applicable.

Consent for publication

Not applicable.

Declaration of conflicting interest

The author(s) declared no potential conflicts of interest with respect to the research, authorship, and/or publication of this article.

Funding statement

The author(s) received no financial support for the research, authorship, and/or publication of this article.

Data availability

The data that support the findings of this study were obtained under a research license from PTV VISSIM and are therefore subject to access restrictions. The data are not publicly available but may be obtained from the corresponding author upon request and with permission from the licensor.

References

1. Liu J, Zhang R, Yan W, Zhao Q, and Guo C. Modeling and simulation of fire evacuation considering guiding factors: a case study of Shenyang subway interchange station. *Simulation* 2024; 100:1053–68.
2. Peng J, Wei Z, Li J, Guo X, and Wang S. Passenger flow bottleneck decongestion in subway stations: a simulation study. *Simulation* 2024; 100:981–95.
3. Chraïbi M, Tordeux A, Schadschneider A, and Seyfried A. Modelling of pedestrian and evacuation dynamics. In: *Complex dynamics of traffic management*. Springer, 2019, pp. 649–669.
4. Helbing D and Molnar P. Social force model for pedestrian dynamics. *Physical review E* 1995; 51:4282–6.
5. Burstedde C, Klauck K, Schadschneider A, and Zittartz J. Simulation of pedestrian dynamics using a two-dimensional cellular automaton. *Physica A: Statistical Mechanics and its Applications* 2001; 295:507–25.
6. Daganzo CF. The cell transmission model: A dynamic representation of highway traffic consistent with the hydrodynamic theory. *Transportation Research Part B: Methodological* 1994 Aug; 28:269–87. DOI: 10.1016/0191-2615(94)90002-7.
7. Daganzo CF. The cell transmission model, part II: Network traffic. *Transportation Research Part B: Methodological* 1995 Apr; 29:79–93. DOI: 10.1016/0191-2615(94)00022-r.
8. Asano M, Sumalee A, Kuwahara M, and Tanaka S. Dynamic cell transmission-based pedestrian model with multidirectional flows and strategic route choices. *Transportation Research Record* 2007; 2039:42–9.

9. Moustaid E and Flötteröd G. Macroscopic model of multidirectional pedestrian network flows. *Transportation Research Part B: Methodological* 2021 Mar; 145:1–23. DOI: 10.1016/j.trb.2020.12.004.
10. Zhang J and Seyfried A. Comparison of intersecting pedestrian flows based on experiments. *Physica A: Statistical Mechanics and its Applications* 2014; 405:316–25.
11. Aghabayk K, Radmehr K, and Shiwakoti N. Effect of intersecting angle on pedestrian crowd flow under normal and evacuation conditions. *Sustainability* 2020; 12, 1301.
12. Feinstein Z, Kleiber M, and Weber S. Stochastic cell transmission models of traffic networks. arXiv preprint arXiv:2304.11654 2023.
13. Flötteröd G and Nagel K. Some practical extensions to the cell transmission model. In: *Proceedings of the 2005 IEEE Intelligent Transportation Systems Conference (ITSC)*. Vienna, Austria, 2005 , pp. 172–177. DOI: 10.1109/ITSC.2005.1520042.
14. Tampère CM, Corthout R, Cattrysse D, and Immers LH. A generic class of first order node models for dynamic macroscopic simulation of traffic flows. *Transportation Research Part B: Methodological* 2011 Jan; 45:289–309. DOI: 10.1016/j.trb.2010.06.004.
15. Flötteröd G and Rohde J. Operational macroscopic modeling of complex urban road intersections. *Transportation Research Part B: Methodological* 2011; 45:903–22.
16. Guo RY, Huang HJ, and Wong S. Collection, spillback, and dissipation in pedestrian evacuation: A network-based method. *Transportation research part B: methodological* 2011; 45:490–506.
17. Hänseler FS, Bierlaire M, Farooq B, and Mühlematter T. A macroscopic loading model for time-varying pedestrian flows in public walking areas. *Transportation Research Part B: Methodological* 2014; 69:60–80.
18. Tak S, Kim S, and Yeo H. Agent-based pedestrian cell transmission model for evacuation. *Transportmetrica A: Transport Science* 2018; 14:484–502. DOI: 10.1080/23249935.2017.1280559.
19. Flötteröd G and Lämmel G. Bidirectional pedestrian fundamental diagram. *Transportation Research Part B: Methodological* 2015 Jan; 71:194–212. DOI: 10.1016/j.trb.2014.11.001.
20. Lilasathapornkit T and Saberi M. Dynamic pedestrian traffic assignment with link transmission model for bidirectional sidewalk networks. *Transportation Research Part C: Emerging Technologies* 2022; 145, 103930.
21. Pohlmann T and Friedrich B. Online control of signalized networks using the Cell Transmission Model. In: *13th International IEEE Conference on Intelligent Transportation Systems*. IEEE, 2010 Sep. DOI: 10.1109/itsc.2010.5625064.
22. Feinstein Z, Plückerbaum J, and Weber S. Extending the Cell Transmission Model for Conflict-Aware Intersection Modeling, Manuscript submitted for publication. 2026.